Acta Materialia 212 (2021) 116931

Contents lists available at ScienceDirect

Acta Materialia

journal homepage: www.elsevier.com/locate/actamat

Full length article

Increased magnetocaloric response of FeMnNiGeSi high-entropy alloys

Jia Yan Law*, Álvaro Díaz-García, Luis M. Moreno-Ramírez, Victorino Franco*

Departmento de Física de la Materia Condensada, ICMS-CSIC, Universidad de Sevilla, P.O. Box 1065, 41080-Sevilla, Spain

ARTICLE INFO

Article history:
Received 16 February 2021
Revised 20 April 2021
Accepted 22 April 2021
Available online 27 April 2021

Keywords:
High-entropy alloys
First-order phase transitions
Magneto-structural transformations
Functional properties
Magnetocaloric effect

ABSTRACT

The search for high-entropy alloys (HEAs), a new class of materials, with high magnetocaloric performance can address the open question about their potential in functional applications. HEAs exist in a vast compositional space but magnetocaloric HEAs typically exhibit modest magnetocaloric response as they undergo second-order magnetic phase transitions. In this work, through a property-directed search approach, FeMnNiGeSi HEAs with varying Ge/Si ratio are found in the large HEA space to exhibit magneto-structural first-order phase transition. Isothermal entropy change as large as 13 J $kg^{-1}K^{-1}$ (for 2.5T) is achieved, which is the largest reported to date for magnetocaloric HEAs. When compared to conventional high-performance magnetocaloric materials, our work is observed to be comparable to many of the conventional systems, closing the gap between magnetocaloric HEAs versus conventional magnetocaloric materials for the first time. This opens a new path for the search of functional materials with the optimal mechanical properties of HEAs.

Introduction

High-entropy alloys (HEAs) are highly considered as a game-changer for designing and developing advanced materials as they have been found exhibiting remarkable mechanical properties, phase stability, wear and corrosion resistance, etc., when compared to conventional alloys [1, 2]. HEAs utilize a multiple principal element alloying concept to yield high configurational entropy of mixing (ΔS_{mix}) unlike the traditional way of alloys design, which is to alloy elements to one or two main constituents. Hence, HEAs are defined with respect to composition (quinary alloy with the composition for each element as 5 – 35 at.%) and entropy (ΔS_{mix} > 1.5 R where R is the gas constant) [1, 2]. While the rapid expansion pace of HEA research enables the development of two generations of HEAs (from first generation equiatomic single-phase HEAs to recent emphasis of second generation multi-phase and/or non-equiatomic HEAs [1]) covering a wide range of compositions, their reports mainly focus on structural applications as shown in a radar chart in Fig. 1. Let us focus on magnetocaloric effect (MCE) as an example of the functional property research as many of the recent functional HEA publications report for magnetocaloric HEAs [3]. MCE is defined as the adiabatic temperature change or isothermal entropy change of a magnetic material induced by the application of a varying magnetic field; thus, it forms the basis of the emergent and environmentally friendly magnetic refrigeration [4]. Hence, there is a growing interest in developing magnetocaloric HEAs and studying their MCE even though their reports are very few compared to structural HEAs. The additional motivation for finding HEAs with relevant magnetocaloric response is twofold:

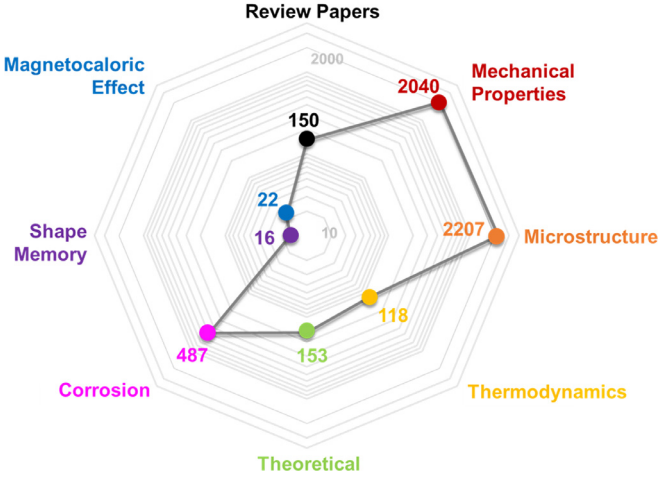

Fig. 1. The number of HEA publications and their different focus, including mechanical properties, microstructures etc. Bibliographic Scopus search was dated up to December 2020 using "high-entropy alloys" and the above-presented labels. .

* Corresponding author.
E-mail addresses: jylaw@us.es (J.Y. Law), vfranco@us.es (V. Franco).

https://doi.org/10.1016/j.actamat.2021.116931

HEAs have a great potential for optimal mechanical properties and most high performing conventional magnetocaloric materials suffer from serious limitations due to their limited mechanical integrity during cycling [4]. The combination of optimal mechanical and functional properties would be a leap forward in the development of more reliable magnetic refrigerators. However, until recently, this approach faced the severe limitation that there was a significant gap between the functionality of magnetocaloric HEAs and that of conventional materials, being this particularly alarming in the case of rare-earth (RE) free HEAs.

Magnetocaloric HEA compositions, similar to the evolution from first → second HEA generation, started from equiatomic compositions until some recent works report on compositions related to the second generation of HEAs [5,6]. Most of the published results mainly focus on the tunability of the transition temperature rather than the magnitude of the magnetocaloric response, which remains considerably lower than that of conventional materials [7–10]. Among the recent results in this area, it is particularly interesting to analyze the influence of the distribution of exchange interactions in HEAs with second order phase transitions [11,12].

Recently, it was shown that a large MCE can be attained in the vast HEA compositional space from a non-equiatomic quinary HEA, $Fe_{22.2}Mn_{22.3}Ni_{22.2}Ge_{16.65}Si_{16.65}$ [5], which exhibited 97% increase in isothermal entropy change (44% increase in refrigerant capacity performance) compared to the notable magnetocaloric HEA $Gd_{20}Dy_{20}Er_{20}Ho_{20}Tb_{20}$ [13]. The possibility of MCE enhancement in HEAs without relying on RE element(s) is surprising, especially taking into account that the previously large MCE values in HEAs were only found for those containing RE in equiatomic contents as these elements intrinsically exhibit large magnetic moments. In addition, it has always been challenging to make a rational search through the vast HEA compositional space so the alloy design of $Fe_{22.2}Mn_{22.3}Ni_{22.2}Ge_{16.65}Si_{16.65}$ HEA was based on property-directed search strategy: identifying alloy compositions with desired behavior as the starting composition and further tune it towards the HEA space. Despite being a promising result, a single HEA composition could not be considered enough to validate the search strategy for MCE-HEAs. In addition, even if there was a significant increase in the isothermal entropy change of that HEA when compared to every other RE-free HEA, the value could not yet reach those of the most notable conventional MCE families. It was still necessary that the search strategy allowed for tunable performance and that the MCE response could therefore be further increased in order to open a new path for the search of HEA magnetocaloric materials.

In this work, a systematic variation of Ge/Si ratio enables a tunable MCE performance of $FeMnNiGe_xSi_{1-x}$ HEAs, which leads to further improvement. The largest MCE found for the alloy with Ge/Si ratio of 0.45:0.55, also closes the gap between magnetocaloric HEAs versus high-performance conventional magnetocaloric materials.

Materials and methods

Ingots of $(FeMnNi)_{66.7}(Ge_xSi_{1-x})_{33.3}$ (where $x = 0.500$, 0.465 and 0.450) were prepared by arc melting pure elements (purity higher than 99.9 wt.%) in an argon-controlled atmosphere. They were flipped and melted four times for homogeneity. Their bulk chemical compositions were characterized from their cross-sections using scanning electron microscope equipped with energy dispersive X-ray spectroscopy (SEM-EDX; FEI^{TM} Teneo). X-ray diffraction (XRD) of the alloys was performed at room temperature using a Bruker D8I diffractometer with Cu-Kα radiation. The sample designation used in this work is denoted by the nominal Ge/Si content of the alloys as $Ge_{0.5}Si_{0.5}$, $Ge_{0.465}Si_{0.535}$ and $Ge_{0.45}Si_{0.55}$ respectively (also tabulated in Table 1).

MCE was indirectly determined, via Maxwell relation, from isothermal magnetic measurements up to 2.5 T performed in a Vibrating Sample Magnetometer by recording isothermal magnetization (M) vs magnetic field (H) curves using a discontinuous protocol [14] in order to erase the memory of the alloy between measurements. This prevents spurious results regardless of the order of the thermomagnetic phase transition [14,15], which has been reported to affect the usage of Maxwell relation to calculate for isothermal entropy change ($\Delta S_{isothermal}$).

The magnetic field dependence of $\Delta S_{isothermal}$ adopts a power law expression [16]:

$$\Delta S_{isothermal} \propto H^n, \tag{1}$$

with an exponent n, both field and temperature dependent, that can be locally calculated as:

$$n = {dln|\Delta S_{isothermal}|}/{dln|H|} \tag{2}$$

The temperature averaged entropy change, *TEC(10)* [17], corresponds to the maximum average of the $\Delta S_{isothermal}$ over a 10 K temperature span and was defined as alternate figure of merit of magnetocaloric materials to avoid the artificially large refrigerant capacity of shallow peaks. For its calculation from literature data without digitizing the whole curves, we had approximated it as:

$$TEC(10) = \frac{1}{10}\max\left(\int_{T-5}^{T+5}\Delta S_{iso}(T')dT'\right) \approx \frac{\Delta S_{isothermal}(T_{pk}-5)+\Delta S_{isothermal}(T_{pk})+\Delta S_{isothermal}(T_{pk}+5)}{3} \tag{3}$$

where T_{pk} is the temperature corresponding to the peak values of $\Delta S_{isothermal}$.

Results and discussion

The XRD patterns and their Rietveld analyses of the studied series are presented in the left panel of Fig. 2 whereby all samples show a single-phase *hcp* structure ($P6_3/mmm$) at room temperature. This is in agreement to the HEA reported in [5]: it shows hexagonal $P6_3/mmc$ structure at room temperature and undergoes a reversible magneto-structural transformation from hexagonal $P6_3/mmc \leftrightarrow$ orthorhombic *Pnma* upon cooling. The scanning electron micrographs and their corresponding backscattered electron images are shown in the right panels of Fig. 2. On a closer look, two phases can be vaguely observed in the micrographs while the phase coexistence is more evident in the corresponding backscattered electron images. The phase composition characterized by SEM-EDX shows two phases without predominant elements: (i) a main phase with composition that corresponds to the nominal and (ii) a minority phase that is Si-depleted. Their details are summarized under Table 1, whereby the measured phase compositions fulfill the operational definitions used for HEAs (systems with more than 4 elements where each elemental composition is of 5–35 atomic% and the configurational entropy of mixing, $\Delta S_{mix} > 1.5$ R where R is the gas constant), especially for the ones containing low density elements [18] (where atomic radius difference, $\delta < 4.5\%$). The single-phase detection from the XRD results could arise from the hexagonal structures with similar lattice parameters of the two regions (observed from SEM-EDX). Such phase discrepancy observations have been reported for HEAs where a single phase was found for both XRD and neutron diffraction results while TEM observations show the presence of secondary phases [19].

Fig. 3 shows the thermomagnetic curves of the HEA series before and after virgin effects. For the virgin curves for low magnetic fields ($\mu_0 H = 0.05$ T) in Fig. 3(a), the samples show that

Table 1
Measured compositions of the studied HEA series with their empirical parameters.

Sample ID	Nominal Composition	Measured Composition		δ (%)[a]	ΔS_{mix} ($Jmol^{-1}K^{-1}$)[b]
$Ge_{0.5}Si_{0.5}$	$(Fe,Mn,Ni)_{66.7}(Ge_{0.5}Si_{0.5})_{33.3}$	Main phase	$Mn_{23.88}Fe_{23.88}Ni_{22.74}Ge_{14.32}Si_{15.18}$	3.2	1.59 R
		Minority phase	$Mn_{28.01}Fe_{18.65}Ni_{23.2}Ge_{20.7}Si_{9.44}$	3.6	1.56 R
$Ge_{0.465}Si_{0.535}$	$(Fe,Mn,Ni)_{66.7}(Ge_{0.465}Si_{0.535})_{33.3}$	Main phase	$Mn_{21.98}Fe_{22.62}Ni_{21.16}Ge_{15.81}Si_{18.43}$	3.3	1.60 R
		Minority phase	$Mn_{23.95}Fe_{19.56}Ni_{20.9}Ge_{22.52}Si_{13.07}$	3.6	1.59 R
$Ge_{0.45}Si_{0.55}$	$(Fe,Mn,Ni)_{66.7}(Ge_{0.45}Si_{0.55})_{33.3}$	Main phase	$Mn_{21.4}Fe_{22.75}Ni_{21}Ge_{16.22}Si_{18.63}$	3.3	1.60 R
		Minority phase	$Mn_{22.99}Fe_{19.33}Ni_{20.93}Ge_{24.21}Si_{12.54}$	3.7	1.59 R

[a] δ is the atomic size difference; constraints of δ for HEAs containing light elements are $\leq$ 4.5%.
[b] ΔS_{mix} is the entropy of mixing; The requirement for HEAs: 1.5 R < $\Delta S_{mix} \leq$ 1.61 R (for quinary alloy) where R is the gas constant.Calculations were based on refs. [18,20,21].

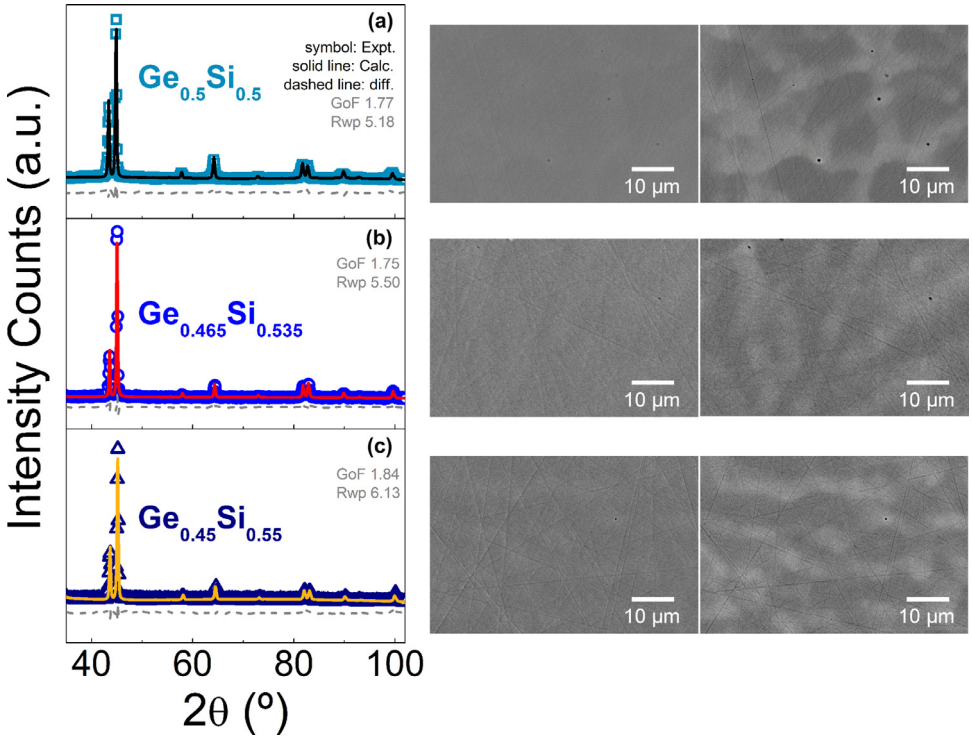

Fig. 2. Left panel to right: XRD data measured at room temperature and their corresponding Rietveld refinement results, scanning electron micrographs, and backscattered electron images of studied series: (a) $Ge_{0.5}Si_{0.5}$, (b) $Ge_{0.465}Si_{0.535}$ and (c) $Ge_{0.45}Si_{0.55}$. (For interpretation of the references to colour in this figure legend, the reader is referred to the web version of this article.)

the low temperature (LT) magnetization phase abruptly increases with temperature (with an increment of ~31.6 A m^2 kg^{-1} at 116 and 125 K) to a higher magnetization phase prior to a gradual decrease at higher temperatures. On the other hand, at higher fields ($\mu_0 H$ = 1.00 T), the samples show that the LT magnetization phase abruptly decreases with temperature to a lower magnetization prior to a gradual decrease with higher temperatures. These observations suggest that the studied HEAs undergo magneto-structural transformation. Upon the virgin measurements, the same magneto-structural transformations are still observed for $Ge_{0.5}Si_{0.5}$ and $Ge_{0.465}Si_{0.535}$ HEAs while $Ge_{0.45}Si_{0.55}$ sample no longer shows the transformation of low magnetization to high magnetization phase for 0.05 T. This is further investigated by their isothermal hysteresis loops, which are presented in Fig. 4.

Fig. 4 shows the first quadrant of isothermal hysteresis loops of the HEA samples, including the initial magnetization curve and the demagnetization (applied magnetic field 0 → 1.5 T → 0). It is observed that both $Ge_{0.5}Si_{0.5}$ and $Ge_{0.465}Si_{0.535}$ HEAs show large effective anisotropy fields at low temperatures. A decrease from ~0.6 T at low temperatures (orthorhombic phase) to ~0.08 T at higher temperatures (hexagonal phase) is observed for $Ge_{0.5}Si_{0.5}$ (~0.5 to ~0.06 T for $Ge_{0.465}Si_{0.535}$). This is due to the reduced symmetry in the lattice which increases the anisotropy. Very small difference between the initial magnetization curve and the loop is noticed up to 1.5 T for 140–147 K and 170–180 K for $Ge_{0.5}Si_{0.5}$ and $Ge_{0.465}Si_{0.535}$ respectively. The observed behavior regarding the change of anisotropy, which also explains the observations in the thermomagnetic data of $Ge_{0.5}Si_{0.5}$ and $Ge_{0.465}Si_{0.535}$ HEAs for 0.05 and 1.00 T in Fig. 3, is similar to that of Ni_2MnGa-based conventional functional materials [22–24]. Coercivity is negligible for all cases. Hence, for these two HEAs, their thermomagnetic phase transitions are: ferromagnetic (FM) martensite → FM austenite → paramagnetic (PM) austenite for both low and high magnetic fields. Conversely for $Ge_{0.45}Si_{0.55}$ HEA, the change in the

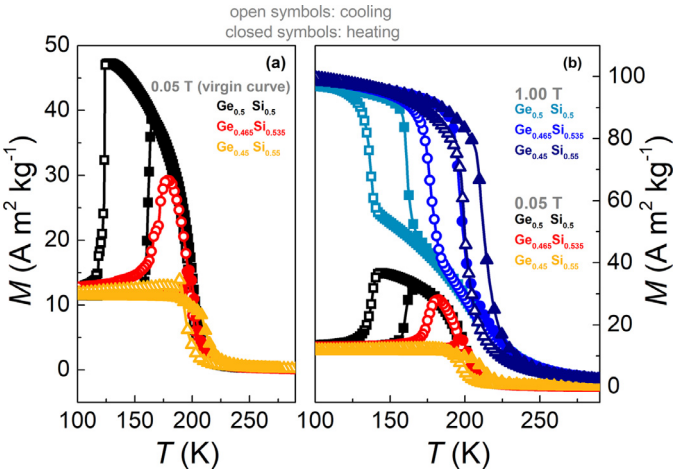

Fig. 3. Thermomagnetic curves of the studied HEAs measured at 2 K min^{-1}: (a) virgin curves and (b) repeated measurements.

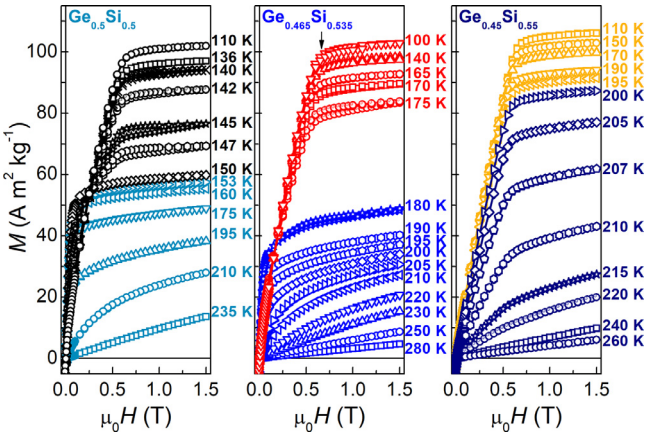

Fig. 4. First quadrant of the isothermal hysteresis loops with initial magnetization curve and demagnetization (measured using a discontinuous cooling protocol). As an example, the arrow indicates the effective anisotropy field for $Ge_{0.465}Si_{0.535}$ at 100 K. (For interpretation of the references to colour in this figure legend, the reader is referred to the web version of this article.)

anisotropic behavior is not observed, which attributes to its thermomagnetic observations in Fig. 3(b), which could indicate that it undergoes magneto-structural transformation of FM martensitic to PM austenitic phase transition or an overlap of phase transitions.

The distinct thermomagnetic and anisotropy behavior of $Ge_{0.5}Si_{0.5}$ and $Ge_{0.465}Si_{0.535}$ HEAs then give rise to an inverse and direct MCE for low and high fields respectively (see Fig. 5(a)). This is easily noticed for $Ge_{0.5}Si_{0.5}$ where a pronounced inverse MCE (black) switches to direct MCE for magnetic fields above 0.6 T (depicted as dark cyan lines). The two types of MCE observed are in agreement with the observations in Fig. 4 whereby magnetization increases with temperature for low fields ($\mu_0 H < 0.27$ T) and decreases with temperature for higher fields. $Ge_{0.465}Si_{0.535}$ HEA exhibits similar thermomagnetic behavior as $Ge_{0.5}Si_{0.5}$ but its inverse MCE for low fields is less evident: subtle inverse MCE can be observed for 0.1 T, which changes to direct MCE with magnetic fields larger than 0.2 T. This agrees with the results in Fig. 3 because its magnetization decreases with increasing temperatures for magnetic fields higher than 0.27 T, thus leading to the direct MCE observed for high fields for $Ge_{0.465}Si_{0.535}$ in Fig. 5(a). For $Ge_{0.45}Si_{0.55}$ HEA, only direct MCE is observed for both low and high magnetic fields, which agrees with its thermomagnetic and hysteresis loop observations. In addition, MCE is observed to shift to higher temperatures as the Ge/Si ratio decreases along the series (~35 K per at.% Ge). Furthermore, a large peak of isothermal entropy change is attained for $Ge_{0.45}Si_{0.55}$ HEA: $|\Delta S^{peak}_{isothermal}|$=13.1 J $kg^{-1}K^{-1}$ at 203 K for 2.5 T. This is the largest MCE reported for magnetocaloric HEAs to date, according to our knowledge (surpasses the highly regarded GdDyErHoTb HEA by a 3.5-fold improvement without using rare-earth elements for this enhancement [13]). The MCE performance of the studied series is further compared with that of reported magnetocaloric HEAs based on $|\Delta S^{peak}_{isothermal}|$, their corresponding peak temperatures (T_{peak}) and *TEC(10)* as shown in Fig. 5(b). The good MCE performance of HEAs mainly corresponds to those compositions containing rare-earth (RE) elements (red spheres) while those without RE are usually with very modest $|\Delta S^{peak}_{isothermal}|$ and *TEC(10)* values (represented by the yellowish spheres). A very large improvement can be observed for our studied FeMnNiGeSi HEAs series (bluish spheres) in comparison to all other magnetocaloric HEAs, especially the RE-free compositions. This can be attributed to the introduction of magneto-structural transformation in the samples, offering another way to improve the functional properties of HEAs other than the typical reliance on RE compositions (where for magnetic properties related cases, they exhibit large magnetic moments, thus are usually used for boosting magnetic performance).

Furthermore, when comparing the performance of magnetocaloric HEAs with conventional magnetocaloric materials that show promising MCE, it can be observed that there is a gap between them (dark red and yellowish regions for HEAs versus dark gray for the well-known $La(Fe,Si)_{13}$ magnetocaloric materials) in Fig. 6. The studied FeMnNiGeSi HEAs (bluish) are located between these materials, merging the gap between HEAs and $La(Fe,Si)_{13}$, which further illustrates the improvement in magnetocaloric properties found and the potential in HEAs for such applications. Furthermore, they are also found to be comparable with several conventional magnetocaloric materials, such as La-manganites, RE Laves phases, RE_5Si_4 and some of the Ni_2Mn-based magnetocaloric materials.

It has been reported for that the power law exponent, n, for the magnetic field dependence of $\Delta S_{isothermal}$ (Eq. (3)) can reveal the order of the phase transitions undergone by the sample [36] as well as the coexistence of overlapping thermomagnetic phase transitions that might not be evidently shown in the MCE curves [40,48,49]. Thus, the exponents n of the studied HEAs are also studied and presented in Fig. 7. The overshoot of n larger than 2 is observed for all three samples, in which occur at temperatures near their T_{peak}. This indicates that the HEAs undergo a first-order thermomagnetic phase transition, which is a criterion verified by many well-known classes of FOPT materials in the literature [5,36–38,40,50–56]. For temperatures above the overshoot above 2, a minimum of n can be observed at ~197.5 K for all the samples before it increases to a plateau of $n = 2$, which indicates the Curie transition and PM states undergone by the alloys with increasing temperatures. This agrees with the observed gradual changes in magnetization with temperatures (above 198 K) in Fig. 2, which indicates the Curie temperature, T_C, of austenitic phase (i.e., the second-order thermomagnetic phase transition). It can also be further observed that $Ge_{0.5}Si_{0.5}$ HEA shows the farthest distance between the T_C and the transition temperature arising from the FOPT (which is the martensitic transition temperature, T_M) among the series. As the Ge/Si ratio decreases, the distance between these *transition temperatures* is tuned nearer to each other, leading to a closer overlap of the T_C and T_M in $Ge_{0.45}Si_{0.55}$, in which its thermomagnetic curves show the behavior similar to FM martensite → PM austenite. The tuning for an overlap of phase transitions could lead to the improved MCE properties of $Ge_{0.45}Si_{0.55}$ among the studied HEA series, whereby it shows an 80% increase compared to $Ge_{0.5}Si_{0.5}$.

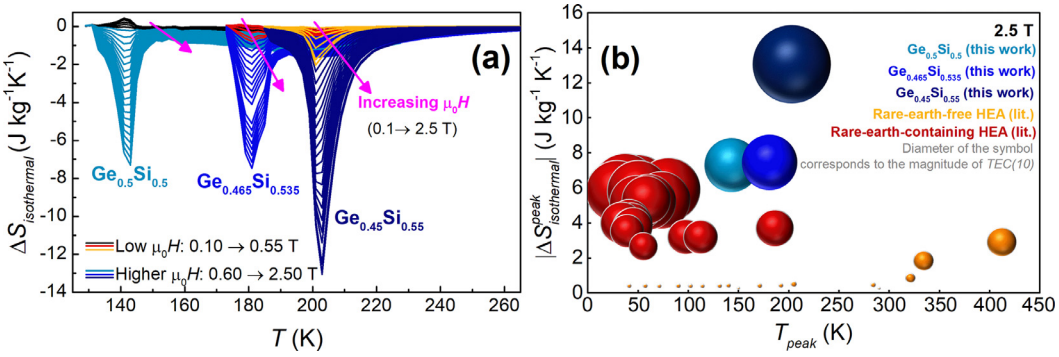

Fig. 5. (a) Isothermal entropy curves of the studied series. (b) MCE performance comparison of studied series with reported magnetocaloric HEAs for 2.5 T. Literature data collected from refs. [6–8, 10,13,25–34]. Each data point represents a single material with a diameter proportional to its *TEC(10)*.

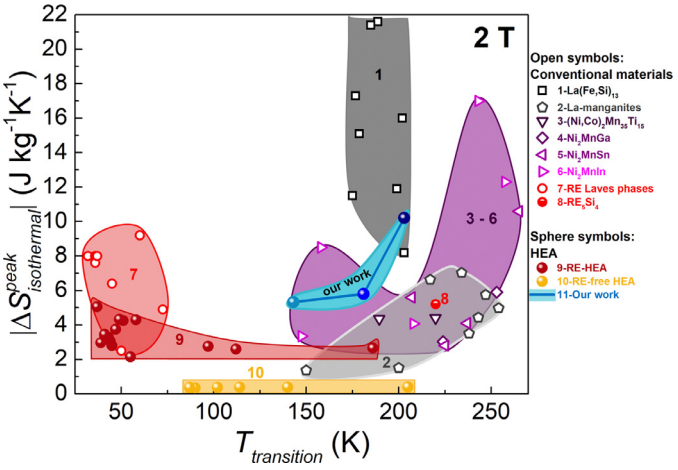

Fig. 6. Peak isothermal entropy change values and transition temperatures of studied series in comparison to high-performance conventional magnetocaloric materials and other magnetocaloric HEAs in the literature for 2 T. Literature data collected from refs. [4–6,8,10,13,25,29–47]. .

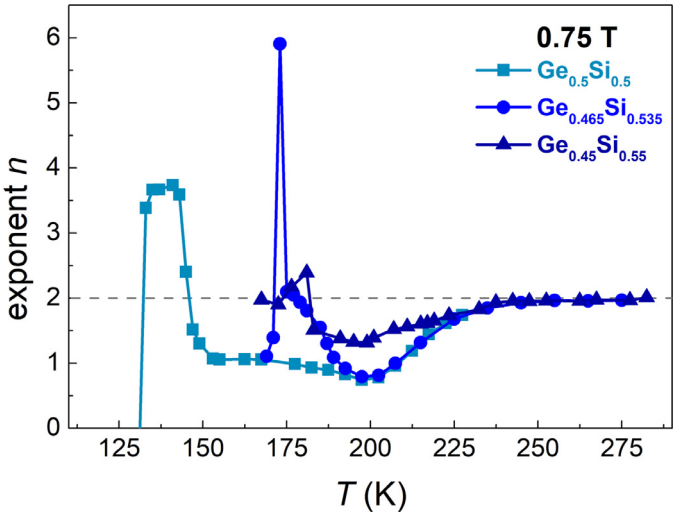

Fig. 7. Temperature dependence of exponent n for the studied HEA series. Dashed line is a guide to the eye for $n = 2$.

Conclusions

Using a property-targeted search approach, a series of $FeMnNiGe_xSi_{1-x}$ HEAs has been designed from the vast HEA compositional space. We demonstrate a significant enhancement of the isothermal entropy change as compared to the magnetocaloric HEAs reported in the literature to date, bridging the gap with the non-HEA high performance magnetocaloric materials. This is achieved by introducing a magneto-structural transformation in HEAs instead of the usual reliance of using rare-earth elements in the compositional designs. Furthermore, by tuning the proximity distance between the magneto-structural transformation temperature and Curie temperature via the variation of Ge/Si ratio leads to a further tuning of the isothermal entropy change. The tunability of this proposed directed search strategy, demonstrating the existence of HEAs with remarkable magnetocaloric properties, opens the path to the search of MCE materials with optimal mechanical properties.

Declaration of Competing Interest

The authors declare no potential conflict of interest.

Acknowledgments

Work supported by AEI/FEDER-UE (grant PID2019–105720RB-I00), US/JUNTA/FEDER-UE (grant US-1260179), Consejería de Economía, Conocimiento, Empresas y Universidad de la Junta de Andalucía (grant P18-RT-746), and Army Research Laboratory under Cooperative Agreement Number W911NF-19–2–0212. JYL acknowledges a grant from VI Plan Propio de Investigación de la Universidad de Sevilla. LMMR acknowledges a postdoctoral fellowship from Junta de Andalucía and European Social Fund (ESF).

References

[1] Y. Zhang, High-Entropy Materials, Springer Singapore, Singapore, 2019.
[2] X. Wang, W. Guo, Y. Fu, High-entropy alloys: emerging materials for advanced functional applications, J. Mater. Chem. A 9 (2) (2021) 663–701.
[3] A. Perrin, D.E. Laughlin, M.E. McHenry, High entropy alloys: magnetocaloric effects, Encyclopedia of Materials: Metals and Alloys, Elsevier, 2021 in press, doi:10.1016/B978-0-12-819726-4.00026-0.
[4] V. Franco, J. Blázquez, J. Ipus, J. Law, L. Moreno-Ramírez, A. Conde, Magnetocaloric effect: from materials research to refrigeration devices, Prog. Mater. Sci. 93 (2018) 112–232.
[5] J.Y. Law, L.M. Moreno-Ramírez, Á. Díaz-García, A. Martín-Cid, S. Kobayashi, S. Kawaguchi, T. Nakamura, V. Franco, MnFeNiGeSi high-entropy alloy with large magnetocaloric effect, J. Alloys Compd. 855 (2021) 157424.
[6] L. Luo, H. Shen, Y. Bao, H. Yin, S. Jiang, Y. Huang, S. Guo, S. Gao, D. Xing, Z. Li, J. Sun, Magnetocaloric effect of melt-extracted high-entropy $Gd_{19}Tb_{19}Er_{18}Fe_{19}Al_{25}$ amorphous Microwires, J. Magn. Magn. Mater. 507 (2020) 166856.
[7] Z. Dong, S. Huang, V. Ström, G. Chai, L.K. Varga, O. Eriksson, L. Vitos, $Mn_xCr_{0.3}Fe_{0.5}Co_{0.2}Ni_{0.5}Al_{0.3}$ high entropy alloys for magnetocaloric refrigeration near room temperature, J. Mater. Sci. Technol. 79 (2021) 15–20.
[8] D.D. Belyea, M.S. Lucas, E. Michel, J. Horwath, C.W. Miller, Tunable magnetocaloric effect in transition metal alloys, Sci. Rep. 5 (2015) 15755.
[9] L. Li, C. Xu, Y. Yuan, S. Zhou, Large refrigerant capacity induced by table-like magnetocaloric effect in amorphous $Er_{0.2}Gd_{0.2}Ho_{0.2}Co_{0.2}Cu_{0.2}$ ribbons, Mater. Res. Lett. 6 (8) (2018) 413–418.

[10] W. Sheng, J.-.Q. Wang, G. Wang, J. Huo, X. Wang, R.-.W. Li, Amorphous microwires of high entropy alloys with large magnetocaloric effect, Intermetallics 96 (2018) 79–83.

[11] A. Perrin, M. Sorescu, M.T. Burton, D.E. Laughlin, M. McHenry, The role of compositional tuning of the distributed exchange on magnetocaloric properties of high-entropy alloys, Jom 69 (11) (2017) 2125–2129.

[12] A. Perrin, M. Sorescu, V. Ravi, D.E. Laughlin, M.E. McHenry, Mössbauer analysis of compositional tuning of magnetic exchange interactions in high entropy alloys, AIP Adv. 9 (3) (2019).

[13] Y. Yuan, Y. Wu, X. Tong, H. Zhang, H. Wang, X.J. Liu, L. Ma, H.L. Suo, Z.P. Lu, Rare-earth high-entropy alloys with giant magnetocaloric effect, Acta Mater. 125 (2017) 481–489.

[14] V. Franco, Determination of the magnetic entropy change from magnetic measurements: the importance of the measurement protocol. https://www.lakeshore.com/docs/default-source/software/vsm/mce-software/determination-of-the-magnetic-entropy-change-from-magnetic-measurements.pdf?sfvrsn=d14f68c1_2, 2014 (accessed 2021).

[15] B. Kaeswurm, V. Franco, K.P. Skokov, O. Gutfleisch, Assessment of the magnetocaloric effect in La,Pr(Fe,Si) under cycling, J. Magn. Magn. Mater. 406 (2016) 259–265.

[16] V. Franco, A. Conde, Scaling laws for the magnetocaloric effect in second order phase transitions: from physics to applications for the characterization of materials, Int. J. Refrig. 33 (3) (2010) 465–473.

[17] L.D. Griffith, Y. Mudryk, J. Slaughter, V.K. Pecharsky, Material-based figure of merit for caloric materials, J. Appl. Phys. 123 (3) (2018) 034902.

[18] M.C. Gao, J.W. Yeh, P.K. Liaw, Y. Zhang, High Entropy Alloys: Fundamentals and Applications, Springer International Publishing, Switzerland, 2016.

[19] W.H. Liu, Y. Wu, J.Y. He, Y. Zhang, C.T. Liu, Z.P. Lu, The phase competition and stability of high-entropy alloys, Jom 66 (10) (2014) 1973–1983.

[20] C. Kittel, Introduction to Solid State Physics, 7th Ed, Wiley, 1996.

[21] A. Takeuchi, A. Inoue, Calculations of mixing enthalpy and mismatch entropy for ternary amorphous alloys, Mater. Trans. 41 (11) (2000) 1372–1378 JIM.

[22] D. Kikuchi, T. Kanomata, Y. Yamaguchi, H. Nishihara, K. Koyama, K. Watanabe, Magnetic properties of ferromagnetic shape memory alloys $Ni_2Mn_{1-x}Fe_xGa$, J. Alloys Compd. 383 (1–2) (2004) 184–188.

[23] F.X. Hu, B.G. Shen, J.R. Sun, Magnetic entropy change involving martensitic transition in NiMn-based Heusler alloys, Chin. Phys. B 22 (3) (2013) 037505.

[24] J. Duan, P. Huang, H. Zhang, Y. Long, G. Wu, Y. Rongchang, Y. Chang, W. Farong, Negative and positive magnetocaloric effect in Ni–Fe–Mn–Ga alloy, J. Magn. Magn. Mater. 309 (1) (2007) 96–99.

[25] M.S. Lucas, D. Belyea, C. Bauer, N. Bryant, E. Michel, Z. Turgut, S.O. Leontsev, J. Horwath, S.L. Semiatin, M.E. McHenry, C.W. Miller, Thermomagnetic analysis of $FeCoCr_xNi$ alloys: magnetic entropy of high-entropy alloys, J. Appl. Phys. 113 (17) (2013) 17A923.

[26] M. Kurniawan, A. Perrin, P. Xu, V. Keylin, M. McHenry, Curie temperature engineering in high entropy alloys for magnetocaloric applications, IEEE Magn. Lett. 7 (2016) 6105005.

[27] K. Sarlar, A. Tekgul, I. Kucuk, Magnetocaloric properties of rare-earth-free $Mn_{27}Cr_7Ni_{33}Ge_{25}Si_8$ high-entropy alloy, IEEE Magn. Lett. 10 (2019) 2109905.

[28] K. Sarlar, A. Tekgül, I. Kucuk, Magnetocaloric properties in a FeNiGaMnSi high entropy alloy, Curr. Appl. Phys. 20 (1) (2020) 18–22.

[29] J.T. Huo, L.S. Huo, H. Men, X.M. Wang, A. Inoue, J.Q. Wang, C.T. Chang, R.W. Li, The magnetocaloric effect of Gd-Tb-Dy-Al-M (M = Fe, Co and Ni) high-entropy bulk metallic glasses, Intermetallics 58 (2015) 31–35.

[30] J. Huo, L. Huo, J. Li, H. Men, X. Wang, A. Inoue, C. Chang, J.Q. Wang, R.W. Li, High-entropy bulk metallic glasses as promising magnetic refrigerants, J. Appl. Phys. 117 (7) (2015) 073902.

[31] J. Huo, J.Q. Wang, W.H. Wang, Denary high entropy metallic glass with large magnetocaloric effect, J. Alloys Compd. 776 (2019) 202–206.

[32] L. Xue, L. Shao, Q. Luo, B. Shen, $Gd_{25}RE_{25}Co_{25}Al_{25}$ (RE = Tb, Dy and Ho) high-entropy glassy alloys with distinct spin-glass behavior and good magnetocaloric effect, J. Alloys Compd. 790 (2019) 633–639.

[33] C.M. Pang, L. Chen, H. Xu, W. Guo, Z.W. Lv, J.T. Huo, M.J. Cai, B.L. Shen, X.L. Wang, C.C. Yuan, Effect of Dy, Ho, and Er substitution on the magnetocaloric properties of Gd-Co-Al-Y high entropy bulk metallic glasses, J. Alloys Compd. 827 (2020) 154101.

[34] C.M. Pang, C.C. Yuan, L. Chen, H. Xu, K. Guo, J.C. He, Y. Li, M.S. Wei, X.M. Wang, J.T. Huo, B.L. Shen, Effect of Yttrium addition on magnetocaloric properties of Gd-Co-Al-Ho high entropy metallic glasses, J. Non-Cryst. Solids 549 (2020) 120354.

[35] V. Franco, J.Y. Law, A. Conde, V. Brabander, D. Karpenkov, I. Radulov, K. Skokov, O. Gutfleisch, Predicting the tricritical point composition of a series of LaFeSi magnetocaloric alloys via universal scaling, J. Phys. D: Appl. Phys. 50 (41) (2017) 414004.

[36] J.Y. Law, V. Franco, L.M. Moreno-Ramirez, A. Conde, D.Y. Karpenkov, I. Radulov, K.P. Skokov, O. Gutfleisch, A quantitative criterion for determining the order of magnetic phase transitions using the magnetocaloric effect, Nat. Commun. 9 (1) (2018) 2680.

[37] L.M. Moreno-Ramírez, C. Romero-Muñiz, J.Y. Law, V. Franco, A. Conde, I.A. Radulov, F. Maccari, K.P. Skokov, O. Gutfleisch, The role of Ni in modifying the order of the phase transition of $La(Fe,Ni,Si)_{13}$, Acta Mater. 160 (2018) 137–146.

[38] L.M. Moreno-Ramírez, C. Romero-Muñiz, J.Y. Law, V. Franco, A. Conde, I.A. Radulov, F. Maccari, K.P. Skokov, O. Gutfleisch, Tunable first order transition in $La(Fe,Cr,Si)_{13}$ compounds: retaining magnetocaloric response despite a magnetic moment reduction, Acta Mater. 175 (2019) 406–414.

[39] K. Liu, S. Ma, C. Ma, X. Han, K. Yu, S. Yang, Z. Zhang, Y. Song, X. Luo, C. Chen, S.U. Rehman, Z. Zhong, Martensitic transformation and giant magneto-functional properties in all-D-metal Ni-Co-Mn-Ti alloy ribbons, J. Alloys Compd. 790 (2019) 78–92.

[40] J.Y. Law, Á.D. García, L.M. Moreno-Ramírez, V. Franco, A. Conde, A.K. Giri, How concurrent thermomagnetic transitions can affect magnetocaloric effect: the $Ni_{49-x}Mn_{36+x}In_{15}$ Heusler alloy case, Acta Mater. 166 (2019) 459–465.

[41] S. Taskaev, K. Skokov, V. Khovaylo, M. Ulyanov, D. Bataev, D. Karpenkov, I. Radulov, A. Dyakonov, O. Gutfleisch, Magnetocaloric effect in cold rolled foils of $Gd_{100-x}In_x$ (x = 0, 1, 3), J. Magn. Magn. Mater. 459 (2018) 46–48.

[42] P.J. von Ranke, V.K. Pecharsky, K.A. Gschneidner, Influence of the crystalline electrical field on the magnetocaloric effect of $DyAl_2$, $ErAl_2$, and $DyNi_2$, Phys. Rev. B 58 (18) (1998) 12110–12116.

[43] H. Zhang, Y.J. Sun, E. Niu, L.H. Yang, J. Shen, F.X. Hu, J.R. Sun, B.G. Shen, Large magnetocaloric effects of RFeSi (R = Tb and Dy) compounds for magnetic refrigeration in nitrogen and natural gas liquefaction, Appl. Phys. Lett. 103 (20) (2013) 202412.

[44] R. Rajivgandhi, J. Arout Chelvane, S. Quezado, S.K. Malik, R. Nirmala, Effect of rapid quenching on the magnetism and magnetocaloric effect of equiatomic rare earth intermetallic compounds RNi (R=Gd, Tb and Ho), J. Magn. Magn. Mater. 433 (2017) 169–177.

[45] P.K. Jesla, J.A. Chelvane, A.K. Nigam, R. Nirmala, Magnetocaloric effect in a multicomponent Laves phase intermetallic compound $Gd_{0.2}Tb_{0.2}Dy_{0.2}Ho_{0.2}Er_{0.2}Al_2$, AIP Conf. Proc. (2020) 030565.

[46] J. Lai, X. Tang, H. Sepehri-Amin, K. Hono, Tuning magnetocaloric effect of Ho_1-Gd Ni_2 and $HoNi_2$-Co alloys around hydrogen liquefaction temperature, Scr. Mater. 188 (2020) 302–306.

[47] R. Rajivgandhi, J.A. Chelvane, A.K. Nigam, S.K. Malik, R. Nirmala, Preservation of large low temperature magnetocaloric effect in metamagnetic intermetallic compounds RCu_2 (R= Gd, Tb, Dy, Ho and Er) upon rapid solidification, J. Alloys Compd. 815 (2020) 152659.

[48] P. Gębara, Á. Díaz-García, J.Y. Law, V. Franco, Magnetocaloric response of binary Gd-Pd and ternary Gd-(Mn,Pd) alloys, J. Magn. Magn. Mater. 500 (2020) 166175.

[49] S.X. Yang, X.Q. Zheng, W.Y. Yang, J.W. Xu, J. Liu, L. Xi, H. Zhang, L.C. Wang, Z.Y. Xu, J.Y. Zhang, Y.F. Wu, X.B. Ma, D.F. Chen, J.B. Yang, S.G. Wang, B.G. Shen, Tunable magnetic properties and magnetocaloric effect of TmGa by Ho substitution, Phys. Rev. B 102 (17) (2020) 174441.

[50] A. Herrero, A. Oleaga, A.F. Gubkin, M.D. Frontzek, A. Salazar, N.V. Baranov, Comprehensive study of the magnetic phase transitions in Tb_3Co combining thermal, magnetic and neutron diffraction measurements, Intermetallics 111 (2019) 106519.

[51] S.K. Pal, C. Frommen, S. Kumar, B.C. Hauback, H. Fjellvåg, G. Helgesen, Enhancing giant magnetocaloric effect near room temperature by inducing magnetostructural coupling in Cu-doped MnCoGe, Mater. Des. 195 (2020) 109036.

[52] P. Gebara, M. Hasiak, Determination of phase transition and critical behavior of the As-cast GdGeSi-(X) type alloys (where X = Ni, Nd and Pr), Mater. (Basel) 14 (1) (2021) 185.

[53] M. Pektas, T. Izgi, H. Gencer, S. Atalay, V.S. Kolat, N. Bayri, Effects of Ru substitution on the structural, magnetic and magnetocaloric properties of $Pr_{0.68}Ca_{0.22}Sr_{0.1}Mn_{1-x}Ru_xO_3$ (x = 0, 0.05, 0.1 and 0.2) compounds, J. Mater. Sci. Mater. Electron. 31 (18) (2020) 15731–15741.

[54] S. Pandey, V. Siruguri, R. Rawat, Effect of Tb substitution in naturally layered $LaMn_2Si_2$: magnetic, magnetocaloric, magnetoresistance and neutron diffraction study, J. Phys. Condens. Matter 32 (3) (2020) 035807 An Institute of Physics Journal.

[55] A. Herrero, A. Oleaga, A.F. Gubkin, A. Salazar, N.V. Baranov, Peculiar magnetocaloric properties and critical behavior in antiferromagnetic Tb_3Ni with complex magnetic structure, J. Alloys Compd. 808 (2019) 151720.

[56] J.Y. Law, V. Franco, A. Conde, S. Skinner, S. Pramana, Modification of the order of the magnetic phase transition in cobaltites without changing their crystal space group, J. Alloys Compd. 777 (2019) 1080–1086.